Magnet Loss Computation for PMSMs Under PWM Supply via Corrected Magnetostatic FEA

Magnet Loss Computation for PMSMs Under PWM Supply via Corrected Magnetostatic FEA

Paolo Ragazzo
Dipartimento Energia Galileo Ferraris
Politecnico di Torino
Turin, Italy
paolo.ragazzo@polito.it

Gaetano Dilevrano
Dipartimento Energia Galileo Ferraris
Politecnico di Torino
Turin, Italy
gaetano.dilevrano@polito.it

Simone Ferrari
Dipartimento Energia Galileo Ferraris
Politecnico di Torino
Turin, Italy
simone.ferrari@polito.it

Gianmario Pellegrino
Dipartimento Energia Galileo Ferraris
Politecnico di Torino
Turin, Italy
gianmario.pellegrino@polito.it

***Abstract*—This paper introduces a method to make magnetostatic simulations applicable for computing the permanent magnet loss in PM synchronous machines. Conventional magnetostatic finite-element analysis simulations fail in modelling the eddy current reaction field, leading to a significant overestimation of magnet loss. Consequently, this study provides a comprehensive post-processing manipulation of the magnetostatic field solution to appropriately consider the impact of the reaction field under sinusoidal and PWM supply. Furthermore, the paper addresses the three-dimensional effect, namely the additional loss due to the eddy currents path on the magnet's axial end-side, which is normally addressed via time-consuming 3D simulations. The proposed method is showcased on a motor having the same dimensions and ratings as the Tesla Model 3 interior PM rear-axle motor, highlighting the magnet loss boost caused by the PWM harmonics. The approach presented in the paper leverages a dedicated formulation based solely on 2D magnetostatic analysis, effectively exceeding the capabilities of conventional 2D transient commercial solvers. The obtained results are compared with the transient solution obtained with the commercial solver Ansys Maxwell.**

***Index Terms*—Permanent magnet synchronous machine, magnet loss, magnetostatic, PWM supply**

I. Introduction

In the context of designing permanent magnet synchronous machines (PMSMs) for traction applications, addressing eddy current losses in the permanent magnets (PMs) presents a significant and ongoing challenge [1] [2]. Although the magnitude of these losses can be relatively small compared to the total machine losses, they remain a compelling concern in the contemporary automotive industry. Indeed, in most cases, the magnet loss represents a strict bottleneck to the motor's continuous performance, as even a minor quantity of heat may represent a substantial temperature rise in a PMSM with no rotor cooling. It is in fact imperative to maintain the PM temperature within a specific limit, typically around 160 °C. This challenge is exacerbated by the use of windings with low number of turns in series (low p.u. inductance) under pulse-width-modulated (PWM) inverter supply: the PWM voltage supply introduces current harmonics that magnify PM losses [3]. However, the trend to increase the switching frequency [4] [5] reduces the machine loss. In addition, dealing with this specific type of loss proves to be particularly critical with standard cooling arrangements, such as liquid cooling jackets around the stator laminations, as the PMs are situated at a considerable distance from the active coolant.

To visualize the impact of temperature on PM characteristics, consider Fig. 1 displaying the BH curve of the NdFeB PM grade N35UH, a widely used type of PM in traction applications. UH stands for the Ultra-High temperature class of sintered NdFeB magnets, with a maximum allowed operating temperature of 180°C. The BH curves illustrate how the PM temperature Θ_{PM} exerts a significant influence.

This paper provides a comprehensive review of magnet loss computation and subsequently introduces a method for computing PM losses based on efficient and straightforward magnetostatic FEA, including off-line evaluation of the reaction field and 3D effects. Reference is made to a PM piece whose dimensions and characteristics are detailed in Tab. I. The results of the paper refer to an interior PMSM similar to the Tesla Model 3 rear-axle traction motor, under both sinusoidal

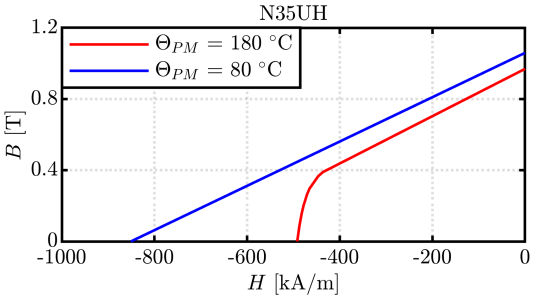

Fig. 1. BH curve of the N35UH, a rare-earth NdFeB PM.

TABLE I
N35UH CHARACTERISTICS AT 20°C AND DIMENSIONS OF THE CONSIDERED PM PIECE.

Material characteristics			
Resistivity	ρ	1.8 10^{-5}	[Ωm]
Relative permeability	μ_r	1.05	
Remanence	B_r	1.2	[T]
Magnetic coercivity	H_c	917	[kA/m]
PM dimensions			
Length	l_m	100	[mm]
Width	w_m	10	[mm]
Height	h_m	3	[mm]

and PWM types of suppl. Last, the results are compared with the reference commercial transient solver Ansys Maxwell, demonstrating the value of the proposed method. The proposed methods are integrated into the open-source design and simulation platform SyR-e [6].

II. MAGNET LOSS MECHANISM

A. Hysteresis loss

The generation of PM losses stems from two primary phenomena, akin to iron losses: hysteresis loops and eddy currents. However, it is worth noting that the contribution of hysteresis to PM losses is notably less significant compared to eddy current losses. For instance, during the demagnetization of PMs, minor hysteresis loops are created, resulting in minimal losses [7]. However, these minor loops are transient in nature and do not exert a significant impact on both PM temperature and machine efficiency. Furthermore, it is crucial to avoid demagnetization to ensure consistent PM performance [8]. That said, the prevailing tendency in the literature to downplay hysteresis losses in PMs and prioritize the examination of eddy current losses is well-founded.

B. Eddy current loss

The eddy current phenomenon according to 2D simulation (i.e. PM of infinite axial length) is depicted in Fig. 2, where the fields and currents are highlighted in the axial view of a PM piece of a PMSM. To understand the phenomenon, references are made to Faraday's law, which expresses that a variable magnetic field induces the so-called eddy currents in a conductor. The induced currents flow in closed loops within the conductors perpendicularly to the imposed magnetic field. Conversely, by Lenz's Law, the eddy current creates a magnetic field B_{eddy} that opposes the change in the magnetic field B that created it. Such a field is referred to as the reaction field and it hinders further formation of eddy currents.
Obviously, the eddy current generates also heat due to the Joule effect since a current flows through a material with a non-null resistivity. An additional phenomenon playing a crucial role is the skin effect, namely the tendency of an alternative current to unevenly distribute among the conductor section, causing higher current density near the surface than in the centre. That said, the skin depth δ is defined as the depth where the current density is just 37% of the value at the

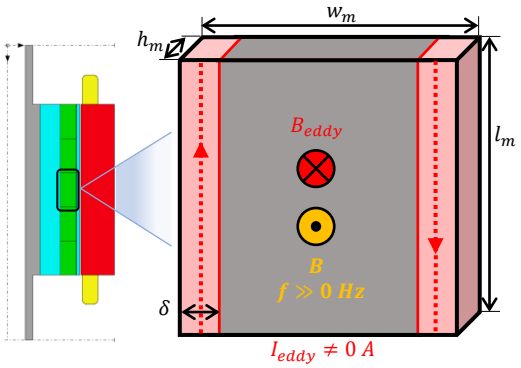

Fig. 2. Axial view of a PM segment in a PMSM. The red bands indicate the eddy currents skin depth δ according to the 2D model, with no end-side closure.

surface. The skin effect is heightened by a frequency rise, as expressed by (1).

$$\delta = \sqrt{\frac{\rho}{\pi f \mu}} \tag{1}$$

Where ρ is the PM resistivity and μ is the material permeability. The skin effect is critical because it reduces the effective cross-section of the conductor, producing higher resistance and thus Joule loss. Last, Fig. 2 is an over-simplified representation of the skin effect phenomenon, indeed, in PMSM the eddy currents in PMs are caused by several rotating fields with different frequencies, thus it often happens that the skin depth is not constant along the PM edges [3]. Also, it can appear more than one eddy current loop in a single PM.

III. REVIEW OF MAGNET LOSS EVALUATION

At this moment, FEA are the most widely used method to accurately estimate PM losses at the design stage [2]. However, the FEA model can be divided into two groups: resistance-limited (magnetostatic) and skin-limited (transient). In the following, these two approaches are discussed and compared.

A. Resistance-limited magnetostatic model

Assuming low frequency, the skin depth is larger than a standard PM width, which erases the reaction field impact. The models that neglect the reaction field are named resistance-limited and are functional to estimate PM loss only related to low harmonics [1] [9]. For instance, consider a PM piece of N35UH reported in Tab I: a frequency equal to around 200 Hz corresponds to a skin depth twice the PM width. Therefore, in this case, neglecting the reaction field is reasonable to assess the PM loss caused by harmonics lower than 200 Hz. Conversely, the significant harmonics in a PMSM extend to over twice the switching frequency, namely around 20-64kHz. That said, the resistance-limited models are deemed ineffective when applied to PMSM.
The method proposed by FEMM [10] is based on magnetostatic simulation [1], thus it belongs to the group of resistance-limited models [11]. In this method, the current density within the PM J_m is calculated as (2).

$$J_m = -\sigma_m \frac{dA}{dt} + J_c \tag{2}$$

where A is the vector magnetic potential, σ_m is the PM conductivity and J_c is the current density required to make the total current in the PM cross-section null. Thus, the PM losses related to the h-th field harmonics are computed by integrating over the PM volume V. Last, the losses of every harmonic are summed to obtain the total loss (3).

$$P_{PM,stat} = 2\sigma_m \pi^2 \sum_h \int_V \left(f_h \cdot J_{m,h}\right)^2 dV \tag{3}$$

B. Skin-limited transient model

The high-frequency harmonics in PMSMs can easily make the skin depth much lower than the PM width, perpetrating a significant reaction field effect that hinders the circulation of eddy currents. The models capable of contemplating the reaction fields are named skin-limited [12] [13]. Yamazaki et al. in [14] retrieved a formulation of the PM losses caused by the eddy current **J** by solving the differential equation of the magnetic field, obtaining the relationship (4). This formulation is valid when a uniform magnetic field H is applied to a PM block with the dimensions defined according to Fig. 2.

$$\begin{aligned} P_{PM} &= \rho\, h_m \int_0^{l_m}\int_0^{w_m} |\mathbf{J}|^2\, dxdy \\ &= \frac{\rho\, h_m\, l_m}{\delta} |H|^2 \frac{sinh\left(\frac{w_m}{\delta_{PM}}\right) - sin\left(\frac{w_m}{\delta_{PM}}\right)}{cosh\left(\frac{w_m}{\delta_{PM}}\right) + cos\left(\frac{w_m}{\delta_{PM}}\right)} \\ &- \frac{16\, w_m\, h_m\, \rho}{\pi} \left|\gamma^2 H\right|^2 \\ &\cdot \Bigg(\sum_{n=0}^{\infty} \frac{(\lambda_n^2 - 2\beta_{ni}^2)\, \beta_{nr}\, \lambda_n^3\, sinh(\beta_{nr} l_m)}{(2n+1)^5\, |\beta_n|^6\, (cosh(\beta_{nr} l_m) + cos(\beta_{ni} l_m))} \\ &+ \sum_{n=0}^{\infty} \frac{(\lambda_n^2 + 2\beta_{nr}^2)\, \beta_{ni}\, \lambda_n^3\, sin(\beta_{ni} l_m)}{(2n+1)^5\, |\beta_n|^6\, (cosh(\beta_{nr} l_m) + cos(\beta_{ni} l_m))} \Bigg) \end{aligned} \tag{4}$$

With

$$\lambda_n = \frac{\pi}{w_m}(2n+1) \tag{5}$$

$$\gamma = \frac{1+j}{\delta} \tag{6}$$

$$\beta_n = \beta_{nr} + j\beta_{ni} = \sqrt{\lambda_n^2 + \frac{2j}{\delta^2}} \tag{7}$$

Regarding FEA models, transient solvers naturally embed the reaction field: commercial FEA such as Ansys Maxwell and JMAG are leading tools in PM loss evaluation. However, for accurate results, 3D FEA are required with significant computational time. It is convoluted to manipulate the field solution of a commercial 2D FEA to make it consider 3D effects. Conversely, the freeware FEMM does not embed the reaction field but it makes it easier to manipulate its field solutions via custom scripts, as done by the proposed method.

IV. Augmented magnetostatic FEA for PM loss

The previous section highlighted the considerable defects of the resistance-limited magnetostatic FEMM model when applied to PMSMs. Therefore, the present section proposes a custom manipulation of the FEMM solution to embed the reaction field and 3D effects.

A. Reaction field effect

The FEMM field solutions are manipulated to account for the reaction field effect with a general analytical approach [15]. From Faraday's Law and Ampere's Law, considering a PM with infinite axial length, the correction factor $k_{PM,RF}$ permits to compute the effective PM losses P_{PM} starting from a magnetostatic estimation $P_{PM,stat}$, namely with no reaction field as the FEMM solutions. Therefore, the $k_{PM,RF}$ (8) is defined as the ratio between P_{PM} (4) and $P_{PM,stat}$ (3).

$$\begin{aligned} k_{PM,RF} &= \frac{P_{PM}}{P_{PM,stat}} = \\ &6 \cdot \left(\frac{\delta_{PM}}{w_m}\right)^3 \cdot \frac{sinh\left(\frac{w_m}{\delta_{PM}}\right) - sin\left(\frac{w_m}{\delta_{PM}}\right)}{cosh\left(\frac{w_m}{\delta_{PM}}\right) + cos\left(\frac{w_m}{\delta_{PM}}\right)} \end{aligned} \tag{8}$$

Where w_m is the PM width, as indicated in Fig. 2 and δ_{PM} is an improved formulation of the skin depth that considers the air gap length $h_{m,air}$ between PMs and rotor flux carriers (9).

$$\delta_{PM} = \sqrt{\frac{\rho}{\pi f \mu}} \cdot \sqrt{\frac{h_m + h_{m,air}}{h_m}} \tag{9}$$

Where h_m is the PM height defined according to Fig. 2. However, the add-on (9) with respect to the original version (1) is a minor adjustment to the skin depth but it can have a non-negligible impact on the PM losses. Indeed, assuming a ratio $h_{m,air}/h_m$ equal to 0.05, δ_m is increased by 2% respect to the simplified δ, causing a significant change on the reaction field coefficient as depicted in Fig. 3. For instance, considering a loss harmonics of 50kHz, a gap of 1mm corresponds to almost twice the PM losses of the nil gap case.
The PM dimensions influence is investigated in Fig. 4, by considering the PM piece of Tab. I and by varying first width and then height, while the gap is fixed. The results in Fig. 4b communicate that the PM height has almost no impact

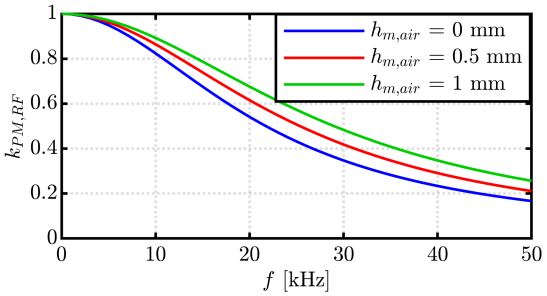

Fig. 3. PM loss correction factor due to reaction field $k_{PM,RF}$ as a function of frequency and air gap height inside the rotor barrier. A N35UH PM 10mm wide is considered.

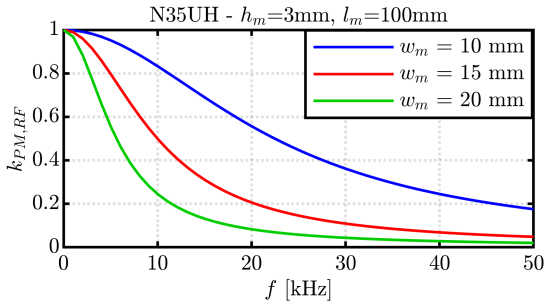

(a)

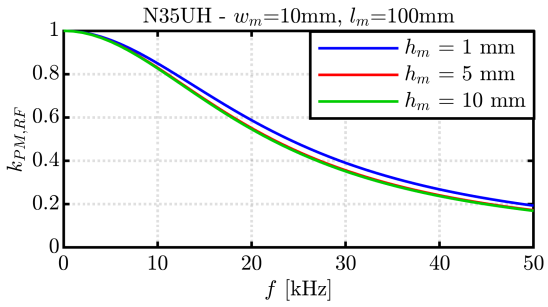

(b)

Fig. 4. PM loss correction factor due to reaction field $k_{PM,RF}$ as a function of frequency and (a) PM width or (b) PM height, both with a gap of 0.1mm.

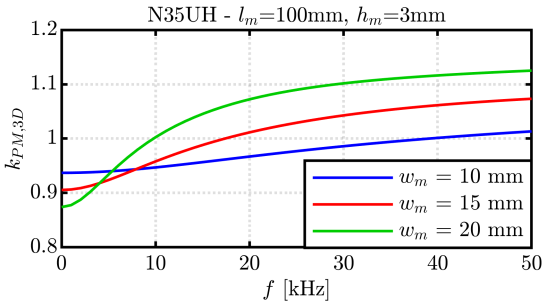

(a)

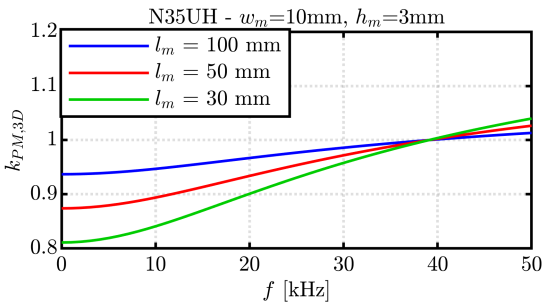

(b)

Fig. 6. PM loss correction factor due to 3D effect $k_{PM,3D}$ as a function of frequency and (a) PM width or (b) PM length, both with a gap of 0.1mm.

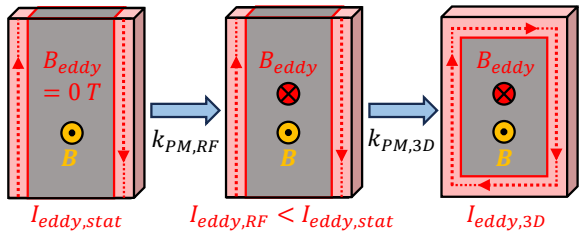

Fig. 5. Augmented model of the eddy current in PMs starting from 2D magnetostatic simulation and then adding the reaction field and 3D effects.

on the correction factor, while the opposite is found for the PM width Fig. 4a. Indeed, the correction factor is boosted by lowering the PM width, which leads to higher specific PM loss. This result is reasonable since PMs with higher w_m produce greater reaction fields due to longer eddy current paths. Conversely, the PM height has no impact, since the axial direction dominates the reaction field phenomenon.

Concerning the segmentation, the present analysis demonstrates that with circumferential segments (i.e. a width decrease) the loss reduction due to the reaction field is attenuated since the eddy current amplitude is reduced.

Notably, the PM loss harmonics at very high frequencies are almost cancelled by the reaction field, with significant benefit on the resulting PM losses. Overall, the discussed coefficient $k_{PM,RF}$ permits to model the reaction field effect in PM with infinite axial length, namely with no eddy current reclosing on the PM axial end-side (second PM piece of Fig. 5).

B. 3D and axial segmentation effect

The 2D simulations fail to model the eddy current path at the axial end-side of the PM, which is displayed on the last PM block in Fig. 5. However, this effect in most cases has a significant influence that forces the machine designers to run time-consuming 3D FEA. Therefore, similarly to what is done with the reaction field, a general analytical approach is employed [15] [16] to retrieve the correction factor $k_{PM,3D}$ (10), which permits to adjust the 2D FEA solution by contemplating the 3D effect.

$$k_{PM,3D} = 1 - \frac{32 w_m}{\pi^5 l_m} \cdot \left(\frac{w_m}{\delta_{PM}}\right)^3 \cdot \frac{cosh\left(\frac{w_m}{\delta_{PM}}\right) + cos\left(\frac{w_m}{\delta_{PM}}\right)}{sinh\left(\frac{w_m}{\delta_{PM}}\right) - sin\left(\frac{w_m}{\delta_{PM}}\right)} \cdot \left(\sum_{n=0}^{\infty} \frac{\left(\lambda_n^2 - 2\beta_{ni}^2\right) \beta_{nr} \lambda_n^3 \, sinh(\beta_{nr} l_m)}{(2n+1)^5 \left|\beta_n\right|^6 \left(cosh(\beta_{nr} l_m) + cos(\beta_{ni} l_m)\right)} + \sum_{n=0}^{\infty} \frac{\left(\lambda_n^2 + 2\beta_{nr}^2\right) \beta_{ni} \lambda_n^3 \, sin(\beta_{ni} l_m)}{(2n+1)^5 \left|\beta_n\right|^6 \left(cosh(\beta_{nr} l_m) + cos(\beta_{ni} l_m)\right)} \right) \tag{10}$$

To understand the impact on the PM losses, the PM piece in Tab I is considered: the PM width w_m and length l_m are varied respectively in Fig. 6a and Fig. 6b. In the first case, the low-frequency PM loss harmonics are decreased by the 3D effect; the fundamental, rotor and stator slots harmonics may fall into this group. Conversely, the high-frequency PM loss harmonics, such as the one related to the PWM, are increased up to 12%. Note that the circumferential segmentation decreases the PM width, resulting in reduced 3D impacts ($k_{PM,3D}$ closer to one). Reasonably, having a wider PM corresponds to longer

paths for the eddy currents on the end side, emphasizing the 3D influence. Conversely, the axial segmentation impact is investigated in Fig. 6b, where a PM length cutback accentuates the 3D effect: the loss harmonics below a certain threshold are lowered with more axial segments, while afterwards they are augmented. Such a threshold occurs when the condition ($\delta = 3 \cdot w_m$) is met, namely when the skin depth equals three times the PM width. This explains why such a threshold is not affected by the PM length change (Fig. 6b), instead, it varies with the PM width (Fig. 6a).
To summarize, the circumferential segmentation pushes towards higher frequencies the limit afterwards the PM losses are worsened by the 3D effect, while the axial segmentation accentuates the 3D impact.

V. Case Study

This section reports example results of PM loss to showcase the proposed procedure and to compare it with the reference commercial software Ansys Maxwell. The motor under analysis is a PMSM with a V-type rotor, similar to the one mounted on the Tesla Model 3 and with the radial cross-section depicted in Fig. 7 and the ratings reported in Tab. II. The benchmark utilizes the rare-earth NdFeB magnet N35UH (Tab. I) with 3 axial segments and unsegmented PM in the circumferential direction. Note that the motor mounted on the Tesla uses instead 4 circumferential segments.
The static PM losses $P_{PM,stat}$, which neglect reaction field and 3D effects, are retrieved by the FEMM field solution by using the formulation (3). Subsequently, the introduced coefficients $k_{PM,RF}$ and $k_{PM,3D}$ are applied to every loss harmonics, turning the initial formulation of the PM losses (3) into (11).

$$P_{PM} = 2\sigma_m \pi^2 \sum_h \left(k_{PM,RF,h} \cdot k_{PM,3D,h} \cdot \int_V \left(f_h \cdot J_{m,h} \right)^2 dV \right) \tag{11}$$

In other words, every PM loss harmonics is multiplied by its respective coefficients $k_{PM,RF,h}$ and $k_{PM,3D,h}$, as depicted in Fig. 8.

A. Sinusoidal supply

First, the PM loss map over a dq current grid is computed under an ideal sinusoidal supply at 4000rpm and at Θ_{PM} = 80°C [17]. This computation utilizes a 10x10 current grid,

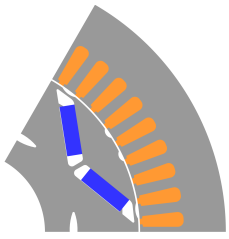

Fig. 7. Radial cross-section of the Tesla Model 3 PMSM.

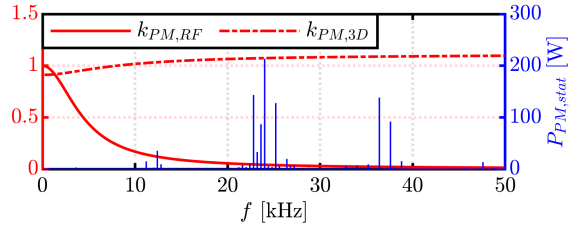

Fig. 8. PM loss harmonics according to the magnetostatic solution of FEMM and the correction factors to account for the reaction field and the 3D effects. The results refer to OP#1.

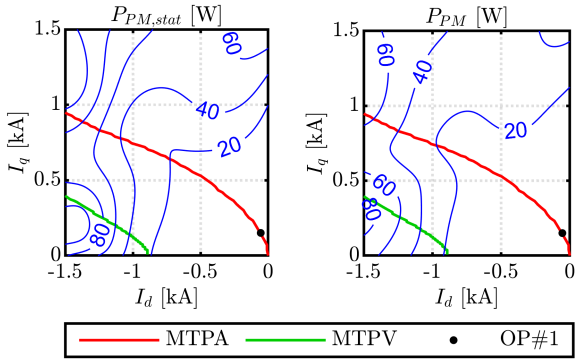

Fig. 9. PM loss contours over the i_{dq} plane for Θ_{PM} = 80°C at 4000rpm and under sinusoidal supply.

incorporating 180 rotor positions spanning 180 electrical degrees (leveraging electrical symmetry). The map is obtained in 90 minutes with a workstation with an Intel Xeon E5-2690 v4, 32GB RAM and 14 cores. For further insights on the loss scaling relative to mechanical speed and the utilization of electrical symmetry, additional details are available in [17]. The Fig. 9 compares the PM loss map obtained with and without the correction factors ($k_{PM,RF}$ and $k_{PM,3D}$), respectively $P_{PM,stat}$ and P_{PM}. Fig. 9 illustrates the substantial influence of both the reaction field and 3D effects, even at fundamental frequencies, indeed, an average reduction of 30% is observed, underscoring the significance of these factors in the overall loss and thermal analysis.

B. PWM supply

When considering non-sinusoidal supply given by a PWM, the impact of the reaction field is magnified with respect to sinusoidal supply, due to greater eddy currents at higher frequencies. Exploiting the dynamic model embedded in SyR-e [6], called syreDrive, the current waveforms under inverter supply are obtained in two operating points (OPs), reported in Tab. II using a switching frequency and a DC voltage equal respectively to 12kHz and 230V. To appreciate the individual impact of each correction factor, the entry $P_{PM,RF}$ is introduced, representing the static solution $P_{PM,stat}$ multiplied solely by the reaction field coefficient, disregarding the 3D effect. Fig. 10 demonstrates the paramount influence of the reaction field coefficient, signifying its profound effect on the PM loss outcomes. Regarding the Ansys bars in Fig. 10,

TABLE II
MOTOR RATINGS AND DATA OF THE SIMULATED OPERATING POINTS.

Machine data				
Stator diameter	D	225		[mm]
Stack length	L	134		[mm]
Circumferential PM segments		1		
Axial PM segments		3		
Operating points		**OP#1**	**OP#2**	
Torque	T	50	200	[Nm]
Speed	n	4000	6000	[rpm]
Current	I	160	660	[Apk]
Current angle	γ	110	152	[° elt]
Condition		MTPA	FW	

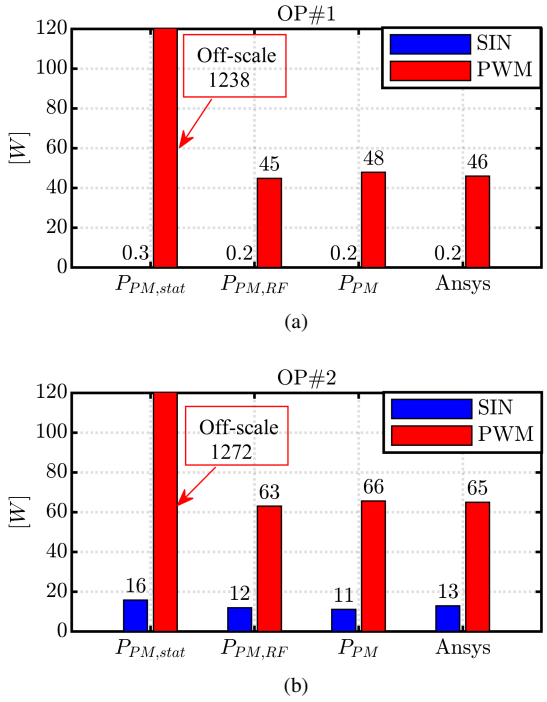

Fig. 10. PM losses in the two analysed OPs: (a) OP#1 and (b) OP#2. $P_{PM,RF}$ consider just the reaction field impact and it neglects the 3D effect.

these results are based on transient Ansys Maxwell simulations of an equivalent model, adopting matching supply, boundary conditions, mesh, and rotor steps. It is essential to note that Ansys does not model the 3D effect, hence its results must be compared with the $P_{PM,RF}$ entry.

VI. CONCLUSION

To summarize, specific adjustment factors are implemented to achieve accurate modelling of PM loss via simple magnetostatic FEA. Among these, the reaction field effect is investigated and its great impact on the resulting loss is explained and demonstrated. Also, the added 3D effect is proved to be less impactful but not negligible. A PMSM for traction application is adopted as a case study, highlighting the value of the novel coefficients: with reference to a transient solver, originally, the magnetostatic simulation results in a massive overestimation of the PM loss, while the added coefficients permit the magnetostatic approach to be accurate and equivalent to a transient simulation.

ACKNOWLEDGMENT

The research has been conducted with the support of Power Electronics Innovation Center (PEIC) of Politecnico di Torino.

REFERENCES

[1] H. Polinder, "Eddy-current losses in the permanent magnets of a PM machine," in *Eighth International Conference on Electrical Machines and Drives*, vol. 1997. Cambridge, UK: IEE, 1997, pp. 138–142.

[2] S. Sirimanna, T. Balachandran, and K. Haran, "A Review on Magnet Loss Analysis, Validation, Design Considerations, and Reduction Strategies in Permanent Magnet Synchronous Motors," *Energies*, vol. 15, no. 17, p. 6116, Jan. 2022.

[3] K. Yamazaki, M. Shina, Y. Kanou, M. Miwa, and J. Hagiwara, "Effect of Eddy Current Loss Reduction by Segmentation of Magnets in Synchronous Motors: Difference Between Interior and Surface Types," *IEEE Transactions on Magnetics*, vol. 45, no. 10, pp. 4756–4759, Oct. 2009.

[4] F. Stella, E. Vico, D. Cittanti, C. Liu, J. Shen, and R. Bojoi, "Design and Testing of an Automotive Compliant 800V 550 kVA SiC Traction Inverter with Full-Ceramic DC-Link and EMI Filter," in *2022 IEEE Energy Conversion Congress and Exposition (ECCE)*. Detroit, MI, USA: IEEE, Oct. 2022, pp. 1–8.

[5] D. Cittanti, F. Stella, E. Vico, C. Liu, J. Shen, G. Xiu, and R. Bojoi, "Analysis, Design, and Experimental Assessment of a High Power Density Ceramic DC-Link Capacitor for a 800 V 550 kVA Electric Vehicle Drive Inverter," *IEEE Transactions on Industry Applications*, vol. 59, no. 6, pp. 7078–7091, Nov. 2023.

[6] G. Pellegrino and F. Cupertino, "SyR-e." [Online]. Available: https://github.com/SyR-e

[7] Y. Aoyama, K. Miyata, and K. Ohashi, "Simulations and experiments on eddy current in Nd-Fe-B magnet," *IEEE Transactions on Magnetics*, vol. 41, no. 10, pp. 3790–3792, Oct. 2005. [Online]. Available: http://ieeexplore.ieee.org/document/1519446/

[8] G. Dilevrano, P. Ragazzo, S. Ferrari, and Pellegrino, "Comparative Design of Ferrite- and NdFeB- PMSMs using the (x,b) Design Plane," in *International Electric Machines and Drives Conference (IEMDC)*, San Francisco, USA, May 2023.

[9] K. Atallah, D. Howe, P. Mellor, and D. Stone, "Rotor loss in permanent magnet brushless AC machines," in *IEEE International Electric Machines and Drives Conference. IEMDC'99. Proceedings (Cat. No.99EX272)*. Seattle, WA, USA: IEEE, 1999, pp. 60–62.

[10] D. Meeker, "FEMM: Finite Element Method Magnetics." [Online]. Available: www.femm.info

[11] ——, "Rotating Losses in a Surface Mount Permanent Magnet Motor." [Online]. Available: https://www.femm.info/wiki/SPMLoss

[12] S. K. Mukerji, M. George, M. B. Ramamurthy, and K. Asaduzzaman, "EDDY CURRENTS IN SOLID RECTANGULAR CORES," *Progress In Electromagnetics Research B*, vol. 7, pp. 117–131, 2008.

[13] K. Yamazaki, M. Shina, M. Miwa, and J. Hagiwara, "Investigation of Eddy Current Loss in Divided Nd–Fe–B Sintered Magnets for Synchronous Motors Due to Insulation Resistance and Frequency," *IEEE Transactions on Magnetics*, vol. 44, no. 11, pp. 4269–4272, Nov. 2008.

[14] K. Yamazaki and Y. Fukushima, "Effect of Eddy-Current Loss Reduction by Magnet Segmentation in Synchronous Motors With Concentrated Windings," *IEEE Transactions on Industry Applications*, vol. 47, no. 2, pp. 779–788, Mar. 2011.

[15] M. Hullmann and B. Ponick, "General Analytical Description of the Effects of Segmentation on Eddy Current Losses in Rectangular Magnets," in *2022 International Conference on Electrical Machines (ICEM)*. Valencia, Spain: IEEE, Sep. 2022, pp. 1757–1762.

[16] K. Yamazaki and A. Abe, "Loss Investigation of Interior Permanent-Magnet Motors Considering Carrier Harmonics and Magnet Eddy Currents," *IEEE Transactions on Industry Applications*, vol. 45, no. 2, pp. 659–665, Mar. 2009.

[17] S. Ferrari, P. Ragazzo, G. Dilevrano, and G. Pellegrino, "Flux and Loss Map Based Evaluation of the Efficiency Map of Synchronous Machines," *IEEE Transactions on Industry Applications*, vol. 59, no. 2, pp. 1500–1509, Mar. 2023.